

Comparison of intermediate-range order in GeO_2 glass: molecular dynamics using machine-learning interatomic potential vs. reverse Monte Carlo fitting to experimental data

Kenta Matsutani,¹ Shusuke Kasamatsu,² and Takeshi Usuki²

¹*Graduate School of Science and Engineering, Yamagata University,
1-4-12 Kojirakawa, Yamagata, 990-8560, Yamagata, Japan*

²*Faculty of Science, Yamagata University, 1-4-12 Kojirakawa, Yamagata, 990-8560,
Yamagata, Japan*

(Dated: 25 September 2024)

The short and intermediate-range order in GeO_2 glass are investigated by molecular dynamics using machine-learning interatomic potential trained on ab initio calculation data and compared with reverse Monte Carlo fitting of neutron diffraction data. To characterize the structural differences in each model, the total/partial structure factors, coordination number, ring size and shape distributions, and persistent homology analysis were performed. These results show that although the two approaches yield similar two-body correlations, they can lead to three-dimensional models with different short and intermediate-range ordering. A clear difference was observed especially in the ring distributions; RMC models exhibit a broad distribution in the ring size distribution, while neural network potential molecular dynamics yield much narrower ring distributions. This confirms that the density functional approximation in the ab initio calculations determines the preferred network assembly more strictly than RMC with simple coordination constraints even when using multiple diffraction data.

I. INTRODUCTION

Network-forming amorphous materials have been actively studied for their structural characterization and understanding because of their excellent mechanical, optical, and transport properties^{1,2}. The atomic arrangements in amorphous materials like silica, germania, zinc dichloride, B_2O_3 , and others show three distinct length scales, which are observed in X-ray or neutron diffraction experiments measuring the structure factor³⁻⁶. The third maximum peak implies the nearest neighbor distance, and the second peak, the principal peak, reflects the size of the local structural motifs such as SiO_2 tetrahedra in silica glass. The first peak, known as the first sharp diffraction peak (FSDP), which correlates with the intermediate-range order (IRO), is proposed to represent the arrangement of these structural motifs⁶. Numerous interpretations of the structural origin of FSDP have been proposed, ranging from quasicrystalline and ring-like structures similar to those found in crystals⁷ to layered structures⁸ and cavities⁹. The difficulty in interpreting FSDP arises from the fact that diffraction experiments provide only one-dimensional reciprocal space structure information. Therefore, computer simulation methods such as reverse Monte Carlo (RMC)¹⁰⁻¹² and molecular dynamics¹³⁻²⁰ have been used to create three-dimensional structural models to obtain information beyond these limitations.

In this work, we focus on GeO_2 glass, which is known as a prototypical oxide network-forming material. The local structural motifs are known as tetrahedral units centered on a Ge atom coordinating 4 oxygen atoms, and these units form a network through the oxygen atom to which the two Ge atoms are coordinated²¹. Structural analysis based on simulations and experiments have been actively conducted for this system^{13-16,22,23}; a brief review and RMC analysis results compared with molecular dynamics and experimental results are given in our previous work²³. However, structural details, especially of IRO, are still under debate. This is partly due to the fact that diffraction experiments only provide one-dimensional information as noted above; as a result, obtaining reasonable structures using the RMC method depends crucially on the initial structure and physical constraints which need to be known beforehand. On the other hand, melt-quench simulations using classical molecular dynamics can often provide a reasonable glass structure, but the agreement of the calculated structure factor with the experimental one is often unsatisfactory. One way to overcome these problems is to combine molecular dynamics and RMC analysis. Previous works have often

performed melt-quench simulations of glass formation using classical molecular dynamics, whose resulting structure is used as the initial structure for subsequent RMC modeling^{24–26}. A downside of this approach is that the final results depend on the RMC method, and the obtained structures may be energetically unfavorable and unphysical.

The above issues may be overcome if an accurate force field was available that can reproduce the structure factors. Towards this end, ab initio molecular dynamics (AIMD) calculates forces acting on atoms on-the-fly based on quantum mechanics principles, but as a result, the calculations are exceedingly computationally demanding; this restricts the simulation timescale to picosecond order and the number of atoms to only a few hundred. Therefore, this technique does not allow for sufficient structural relaxation of the glass, and the simulation cell size is too small (typically less than 1000 Å³) to observe IRO (the correlation length of IRO is proposed to be 10 Å to 20 Å^{4,27–29}).

In the last few decades, a possible solution to this issue has emerged in the form of machine learning potentials, which have been rapidly developed and successfully applied to a wide variety of materials^{30–32}. Unlike classical interatomic potentials, which have analytical forms based on physics and chemistry viewpoints, machine learning potentials rely on no such physical/chemical intuition and are comprised of neural networks^{33,34}, Gaussian process^{35,36}, tensor expansion³⁷, etc. These functional forms are fit to (or, in machine-learning terminology, trained on) ab initio energy and force data. This method offers tremendous computational cost advantages over ab initio molecular dynamics while preserving the accuracy of the reference datasets. It is applicable to diverse systems, such as phase change materials, that require an appropriate description of bond formation and breakage³⁸. We have taken this route in this work and constructed neural network potentials for GeO₂ glass, evaluated its accuracy, and investigated the resulting glass structure.

Even if we are able to obtain reliable three-dimensional structural models using the above-discussed method, a challenging task remains in interpreting the intermediate range order in glass systems. In the past, the bond angle, dihedral angle distribution, and ring size distribution^{39–42} have been used to characterize the intermediate-range order in glass. The former methods represent 3- or 4-body correlations and can describe correlations beyond the nearest neighbor. The latter method can capture more extended structural features based on chemical bonds. While conventional ring analysis achieves some success, it is based on size distribution and neglects ring shape and length scale information. Some re-

searchers have proposed the calculation method and definition of ring shape to overcome these limitations^{6,20,26}. In recent years, another purely mathematical method called persistent homology, which was developed in the 2000s as a tool for analyzing topological features in multiscale data, has been applied to atomistic structures. Persistent homology is one of the fundamental concepts of topological data analysis (TDA) and is widely used in the investigation of glass structures as a tool for extracting structural features beyond local structural motifs. A review of the concepts and applications can be found in refs.^{18,43,44}. We apply these recent developments to investigate the IRO of the glass structure obtained using NNP-MD and RMC modeling.

This paper is organized as follows. The main methods used, such as molecular dynamics and analysis details, are described in the Methods section. The Results and Discussion section focuses on the dependence of local and intermediate order in GeO₂ glass on the neural network potentials molecular dynamics (NNP-MD) results compared to RMC analysis. The conclusion section summarizes this work.

II. METHODOLOGY

A. Training data collection and construction of force field

All AIMD calculations were conducted by Vienna Ab initio Simulation Package⁴⁵ to generate datasets for NNP training. The cutoff energy of the plane wave basis set was 289.8 eV, and the k -point sampling used only the Γ point. The self-consistent-field energies were converged to within 10^{-5} eV. The projector augmented wave method was used to describe electron-ion interactions and the standard density functional approximation Perdew, Burke, and Ernzerhof (GGA-PBE)⁴⁶. A melt-quench process was simulated in AIMD using GGA-PBE with a 96-atom model to obtain glass structure from crystal. The glass and crystal structure under isotropic pressure were also simulated. A small amount of data with different stoichiometries (Ge₃O and GeO₃) are also calculated to prevent phase separation in the NNP-MD³⁸. The training dataset was then extracted from those simulation trajectories, which finally contained 1870 structures; the details of the dataset are described in Table I. Then, we recalculated the extracted 1870 data with a cutoff energy of 500 eV and a k -point sampling of 2 2 2 to obtain high-quality energy and interatomic force data for training the

NNP.⁴⁷ The self-consistent-field energies were converged to within 10^{-6} eV. All molecular dynamics calculations are performed using Nosé-Hoover thermostat under NVT conditions. To confirm whether the learning of NNP had progressed properly, we performed an additional AIMD of the quenching process and collected 200 structures as a test data set. The calculation parameters were the same as those described above.

We employed SIMPLE-NN code⁴⁸ for the generation of our neural network potentials from the above dataset, which is separated into training and validation data with a ratio of 9:1. The structure of neural networks is 70-30-30-1. We employed atom-centered symmetry functions^{30,33,49} as the descriptors, which consisted of 16 radial and 54 angular components ($G2$ and $G4$), and the cutoff radius is 6.0 Å. The specific parameters for each of the symmetry functions are the same as those in Ref. 38 and 50. The loss function is defined as the sum of RMSE for total energy and force. The network was optimized by Adaptive Momentum Estimation⁵¹ (Adam) with 0.001 learning rate, and the batch size was set to 10.

B. Modeling procedure

NNP-MD simulations of glassy GeO_2 were performed using the Large-scale Atomic/Molecular Massively Parallel Simulator (LAMMPS^{52,53}). Firstly, the structure was extracted from the trajectory of an AIMD simulation of liquid GeO_2 consisting of 120 atoms, and each side of the structure was tripled to create a system of 3240 atoms. Then, the extended model served as the initial structure and was maintained at 2500 K, using the trained NNP with Nosé-Hoover thermostat under NVT conditions for 1 ns. Subsequently, all models were quenched to 300 K over a period of 1 ns (cooling rate 2.3 K/ps). The obtained glass structures were held at room temperature and zero pressure for 1 ns. The above procedure was repeated independently three times to obtain three glass structures for evaluating the variation of the calculated quantities.

Five glassy GeO_2 models containing 3240 atoms (Ge 1080 and O 2160 atoms, respectively) were also prepared using the RMC++ code¹¹. The initial structure was generated by randomly arranging atoms into cubic cells under periodic boundary conditions by hard sphere Monte Carlo; the number density was set to that measure by experiment at ambient conditions. The RMC modeling was performed based on structure factors from the neutron diffraction experiment with isotopic substitution⁵⁴. Coordination constraints around Ge

TABLE I. Summary of the training dataset. The first column describes the molecular dynamics calculation with respect to the trajectory, and the second column shows how the structures were extracted from those trajectories. The third describes the number of structures.

	Extracted structures from MD trajectory	Number of structures
crystal (300 to 3000 K)	Every 1 ps from 100 ps MD	100
liquid (3000 K)	Every 50 fs from 25 ps MD	500
quench (3000 to 1000 K)	Every 1 ps from 100 ps MD	100
quench (1000 to 300 K)	Every 350 fs from 35 ps MD	100
glass (0.0682 \AA^{-3} to 0.0796 \AA^{-3})	Every 20 fs from 1 ps MD	50
glass (0.0796 \AA^{-3} to 0.0936 \AA^{-3})	Every 20 fs from 1 ps MD	50
glass (0.0936 \AA^{-3} to 0.1073 \AA^{-3})	Every 20 fs from 1 ps MD	50
glass (0.0682 \AA^{-3} to 0.1073 \AA^{-3})	Every 10 fs from 500 fs MD	50
glass (0.0682 \AA^{-3} to 0.0448 \AA^{-3})	Every 20 fs from 1 ps MD	50
crystal (0.0682 \AA^{-3} to 0.0796 \AA^{-3})	Every 50 fs from 10 ps MD	200
crystal (0.0796 \AA^{-3} to 0.0936 \AA^{-3})	Every 50 fs from 10 ps MD	200
crystal (0.0936 \AA^{-3} to 0.1073 \AA^{-3})	Every 50 fs from 10 ps MD	200
crystal (0.0682 \AA^{-3} to 0.1073 \AA^{-3})	Every 5 fs from 1 ps MD	200
liquid Ge_3O (0.0682 \AA^{-3})	Every 50 fs from 500 fs MD	10
liquid GeO_3 (0.0682 \AA^{-3})	Every 50 fs from 500 fs MD	10

atoms are used to avoid zero-to-three-fold coordinated Ge, which are the same constraints used in our previous work²³ to avoid unphysical local structures. In this work, we additionally introduced coordination constraints around O atoms, which are used to prevent zero- and singly-coordinated O atoms.

C. Ring analysis

Here, we briefly describe the conventional ring definitions, which are used widely in the characterization of glass structures beyond short-range order. The first ring definition which mainly targeted SiO_2 glass was proposed by King in 1967³⁹; she defined a ring as the shortest path between two of the nearest neighbors of a given atom. This definition stems from the

network of tetrahedral units. Using the same shortest path algorithms, Guttman proposed a different ring definition for silica⁴⁰. This defines a ring as the shortest path that comes back to a given atom from one of its nearest neighbors. It is known that sometimes there are large rings that are detected by King’s definition but not by Guttman’s definition. Guttman’s rings can be seen as a subset of King’s rings from this point of view. Another definition, known as primitive ring⁵⁵, defines a ring as one that cannot be broken down into two smaller rings. For the characterization of each GeO_2 glass structure, we chose the above three ring definitions implemented by SOVA software⁵⁶.

The ring analysis has been widely used to characterize glass structures, but the analysis ignores differences in the ring shape and length. Recently, ring shape characterization has been proposed^{6,20,26}, and in this study, we used the method proposed by Shiga²⁶, which is briefly described below. The method focuses on two parameters called roundness and roughness, both of which are easily calculated based on the eigenvectors and eigenvalue of the variance-covariance matrix of the atomic configurations composing the ring. The first eigenvector indicates the direction of the largest variance of those atom configurations. The second eigenvector represents the maximum variance perpendicular to this vector. In addition, the third eigenvector implies the maximum variance perpendicular to these vectors. Therefore, the shape of the ring can be measured by the proportion of these vectors.

D. Persistent homology

In addition to ring analysis, persistent homology (PH), which is implemented in the Homcloud software package⁴⁴, is used to characterize the geometrical features within our models. PH analysis, based on the mathematical subject of algebraic topology, is a recently proposed tool for analyzing n -dimensional holes in the given data set, such as atomic configurations generated by molecular dynamics and reverse Monte Carlo analysis. Theoretical details and applications of persistent homology can be found in the literature^{43,44}; in this section, we will briefly outline how it is calculated. Simply put, this method identifies holes in the data and describes the structure of one-dimensional holes, namely rings. Firstly, a sphere with a common radius is placed at the coordinate of each atom regardless of the atomic species. Secondly, these radii are gradually increased, causing the spheres to overlap and generate new edges, gradually forming a ring. The time at which a ring is generated is recorded as

its birth, corresponding to the horizontal axis in a persistence diagram (PD). As the radii continue to increase, the spheres further continue to overlap and extinguish the ring, which is recorded as its death, corresponding to the vertical axis in the PD. This process can be applied to the atomic configurations, allowing us to obtain a persistence diagram of the entire system, representing the rings and cavities embedded in the atomic configuration. We note that PD diagrams are often constructed by using the square of the radii according to conventions in computational geometry and TDA⁴⁴, and we also use this convention in presenting our data. This work will only focus on the one-dimensional holes which corresponds to rings.

III. RESULTS & DISCUSSION

A. Validation of neural network potential

First, we investigated the quality of the generated NNP using the test dataset. We ran AIMD simulations of the quenching process from 3000 to 300 K on a structure (96 atoms) independent of the training data, extracted the instantaneous structure every 10 ps, performed calculations to improve the accuracy of the AIMD calculations as well as the training data set, and obtained 200 structures as a test data set. In Figure 1, the energies predicted by the NNP are plotted against the AIMD energies of the test set. We can see that the predicted energies of our NNP are in good agreement with the reference AIMD energies, and the RMSE is 7.923 meV/atom, which is within acceptable values comparable to the literature³⁸. Thus, the NNP have the capability to correctly describe interactions between atoms from liquid to glass in GeO₂.

B. Two-body correlations

In the previous section, we confirmed that the generated NNP is numerically well-trained. This NNP was used to perform melt-quench simulations in the 3240-atom model to obtain glass structures. The structure factor is compared to RMC results in Fig 2. The structure factors calculated from 3 independent NNP-MD trajectories are almost identical as evident from the very thin 95 % confidence interval. In general, good agreement between the NNP-MD and RMC models is observed in the heights and positions of prominent peaks in the

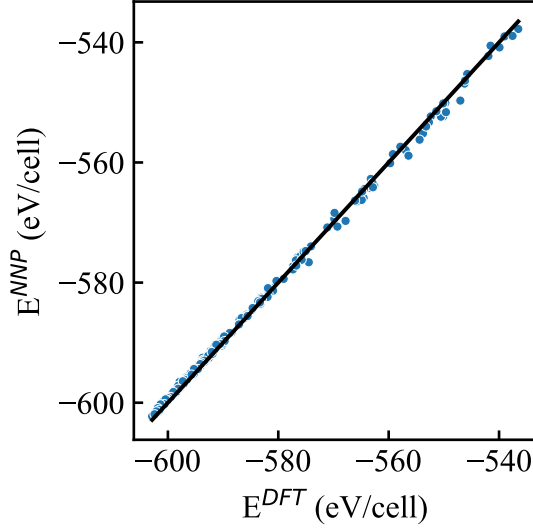


FIG. 1. Comparison between ab initio calculation and NNP on the total energies for the test dataset.

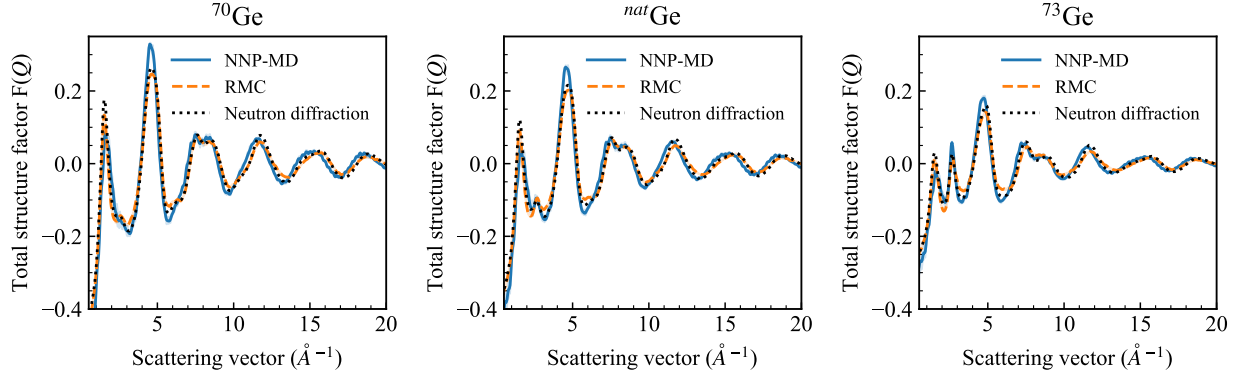


FIG. 2. The comparison between NNP-MD, RMC, and neutron diffraction experiment⁵⁷ of the total structure factors $^{70}F(Q)$, $^{nat}F(Q)$, and $^{73}F(Q)$ for GeO_2 glass. The shaded regions indicate a 95 % confidence interval.

structure factor. However, upon closer observation, it is seen that the RMC models exhibit a slightly higher FSDP which is closer to experiment than the NNP-MD models. On the other hand, the region around the so-called principal peak at $\sim 2.64 \text{ \AA}^{-1}$ is reproduced better by NNP-MD. There are subtle differences in other peaks as well, but in general, the experimental structure factor, RMC models, and NNP-models are in good agreement with each other. The same can be said for the partial structure factors from RMC and NNP

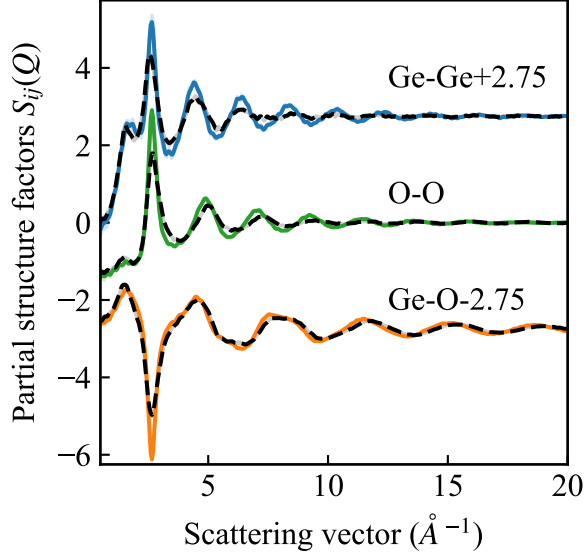


FIG. 3. The comparison of the Faber-Ziman structure factors with NNP-MD (solid lines) and RMC (dashed lines). The shaded regions imply a 95 % confidence interval.

modeling, although the peaks are more slightly more diffuse for the RMC models (Fig. 3).

C. Local coordination environment

The coordination numbers around Ge and O atoms are tabulated in Table II. From this table, we can see that all of our models form a prototypical network structure in which tetrahedral units are cross-linked by O atoms. However, the NNP models exhibit a stronger inclination towards 4-coordination around Ge atoms and 2-coordination around O atoms compared to the RMC models.

TABLE II. The coordination environment around each atom.

	Around Ge				Around O					
	4-fold	5-fold	6-fold	average	1-fold	2-fold	3-fold	4-fold	5-fold	average
GGA-PBE	98.210	1.790	0.000	4.018	0.000	99.090	0.895	0.015	0.000	2.009
RMC	96.444	3.556	0.000	4.036	0.000	98.222	1.778	0.000	0.000	2.018

The bond angle distribution, which is an indicator of three-body correlations, is widely used to describe geometric features in glass structures beyond two-body correlations. Here,

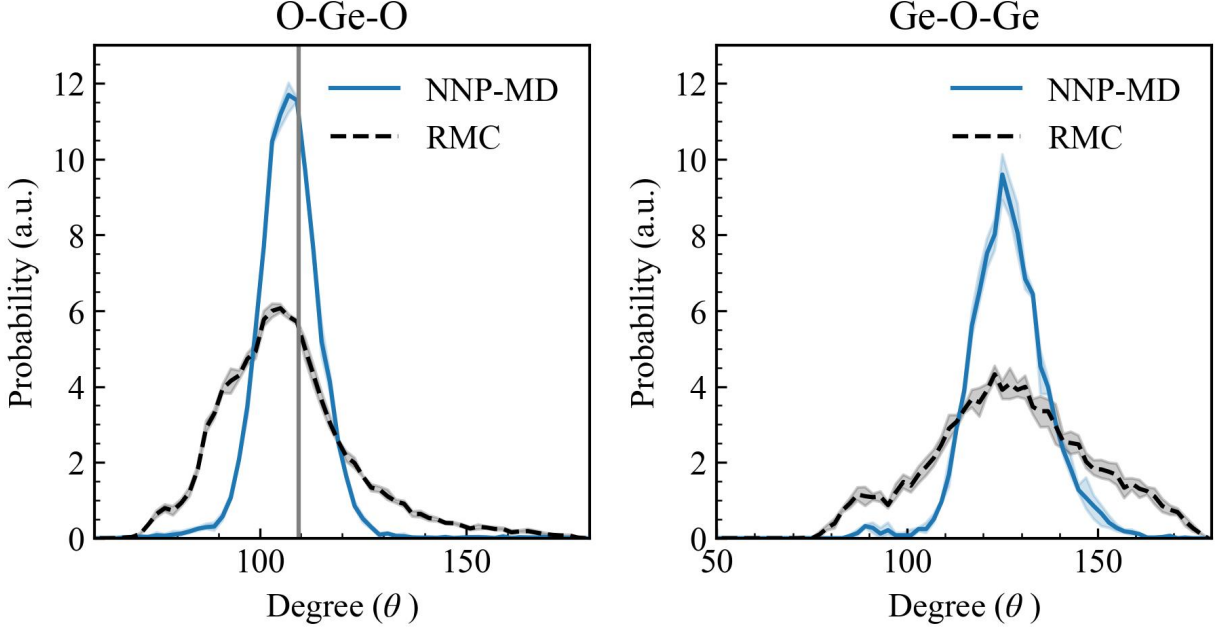


FIG. 4. The bond angle distributions of structure models from reverse Monte Carlo analysis and NNP-MD. The shaded regions indicate a 95 % confidence interval. The gray vertical lines indicate ideal intra-tetrahedral angles.

we calculated the intra- and inter-polyhedral bond angle distributions (O-Ge-O and Ge-O-Ge) for each structure model (Fig. 4). The peak in the intra-polyhedral (O-Ge-O) bond angle distribution for both NNP and RMC models at around 109.5° indicates the existence of tetrahedral units. However, the O-Ge-O distribution for the RMC model has a much broader peak than that of NNP, indicating the higher abundance of distorted tetrahedral units. The interpolyhedral bond angle distributions (Ge-O-Ge) also show broader peaks in the RMC models, but the peak position at $\sim 125^\circ$ is roughly in agreement between the RMC and NNP models. The shoulder around 90° to 100° is present in both models as well, which correspond to chemical bonds between edge-sharing units or distorted units. This is in line with the general trend of the RMC method to result in broader peaks compared to AIMD⁵⁸.

D. Rings

The ring size distribution analysis has been widely used to characterize glass structure beyond two- or three-body correlations. This study employed King’s, Guttman’s, and primitive ring criteria to characterize intermediate-range order in GeO_2 glass to clarify the structural difference between RMC and NNP-MD structural models. Figure 5 shows the average ring size distributions based on three ring criteria of the NNP and RMC structural models. All ring size distributions of RMC are broader than NNP-MD in this study; the ratio of 4- and 6-membered rings as well as the ratio of 16-, 14-, and 18-membered rings according to King’s, Guttman’s, and primitive ring criteria, respectively are larger than NNP-MD, and the peaks in the ring size distributions are also shifted to slightly larger rings in the RMC model. The behavior described above show the same trends as in the interpolyhedral bond angles (Figure 4). The peak around 90° corresponds to the presence of edge-sharing units, corresponding to 4-membered rings in the ring size distribution analysis, and the broad shoulder around 150° to the larger rings that we do not observe in the NNP-MD results. We note that a previous RMC analysis²² reported even larger fractions of 6- and 7-membered rings (they counted only Ge atoms in a ring structure, so 6- and 7-membered rings in previous work mean 12- and 14-membered rings). These differences may be due to the different coordination constraints, as they only allow the existence of 4-fold Ge atoms and 2-fold O atoms in the previous RMC modeling, i.e., there are only corner-sharing units in their structural model. In our RMC models, however, the existence of edge-sharing units and 5-fold Ge and 3-fold O atoms is allowed based on the observation that these structural units exist in AIMD and NNP-MD results.

Figures 6 and 7 show the ring shape characterization of our NNP and RMC models based on the three ring definitions. Ring shape distributions for each ring definition are essentially the same for the roundness and roughness parameters. For further analysis, we calculated the roundness and roughness for each ring size (Figures 8 and 9). The results showed no significant differences, except for the smaller rings (6- and 8-membered rings). The RMC structures exhibit lower roundness values for the 6- and 8-membered rings compared to the NNP structures. Conversely, the RMC structures show higher roughness values for the 6-membered rings. This behavior may be attributed to the RMC’s tendency to produce a more random structure.

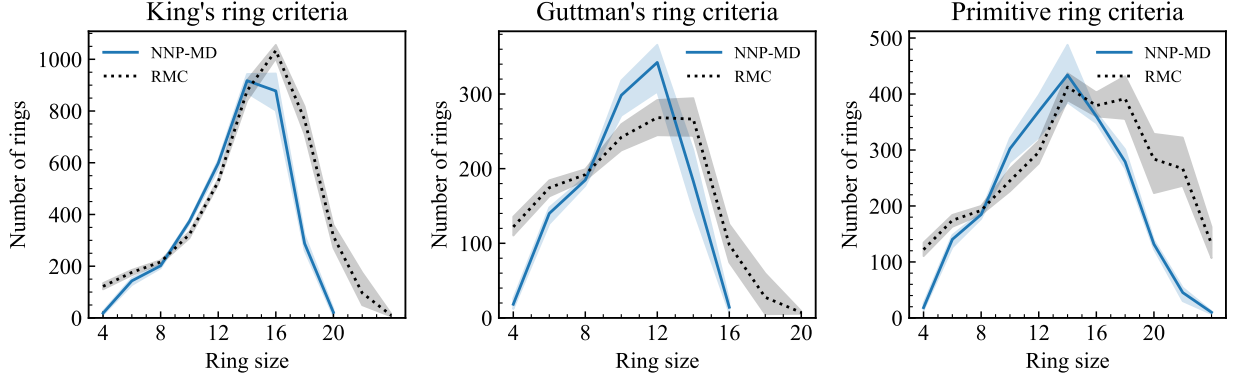


FIG. 5. The ring size distributions of NNP models and RMC models. The number of each ring is normalized by the total number of atoms. The shaded regions imply a 95 % confidence interval.

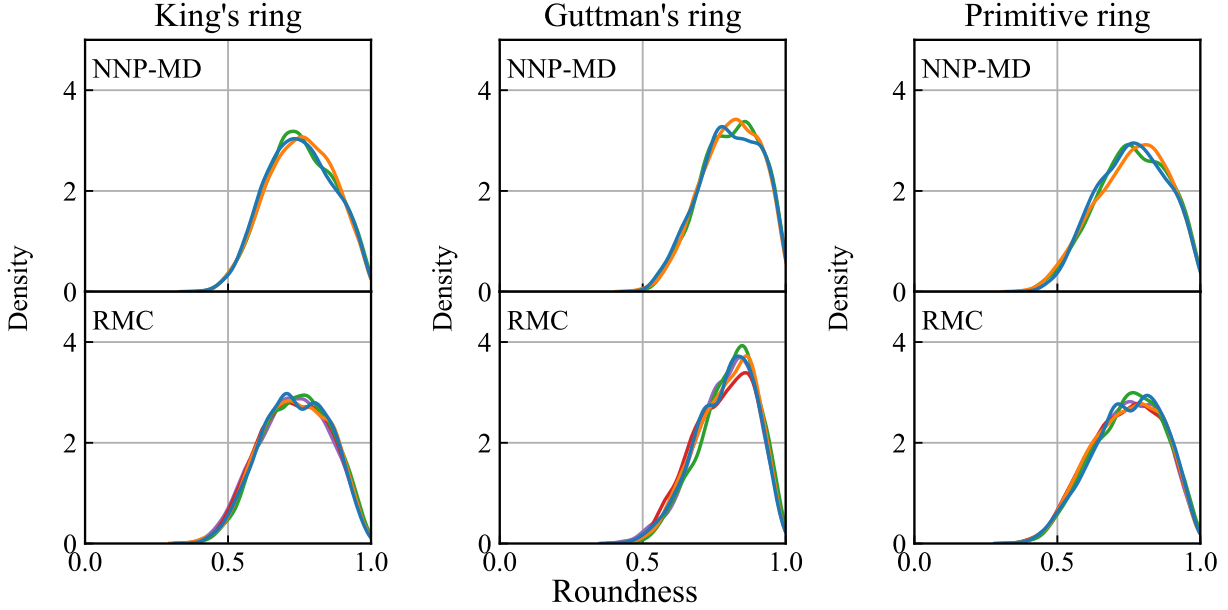


FIG. 6. Kernel density estimate plots of the roundness compared between NNP–MD and RMC using three ring definitions. Here, we present results for each model realization, unlike previous figures where averages of independently generated models are presented.

E. Persistent homology

Figure 10 compares the persistence diagrams obtained by topological data analysis based on RMC and NNP models. Those persistence diagrams imply various ring distributions and the geometrical difference between our models. We can see that the island of birth

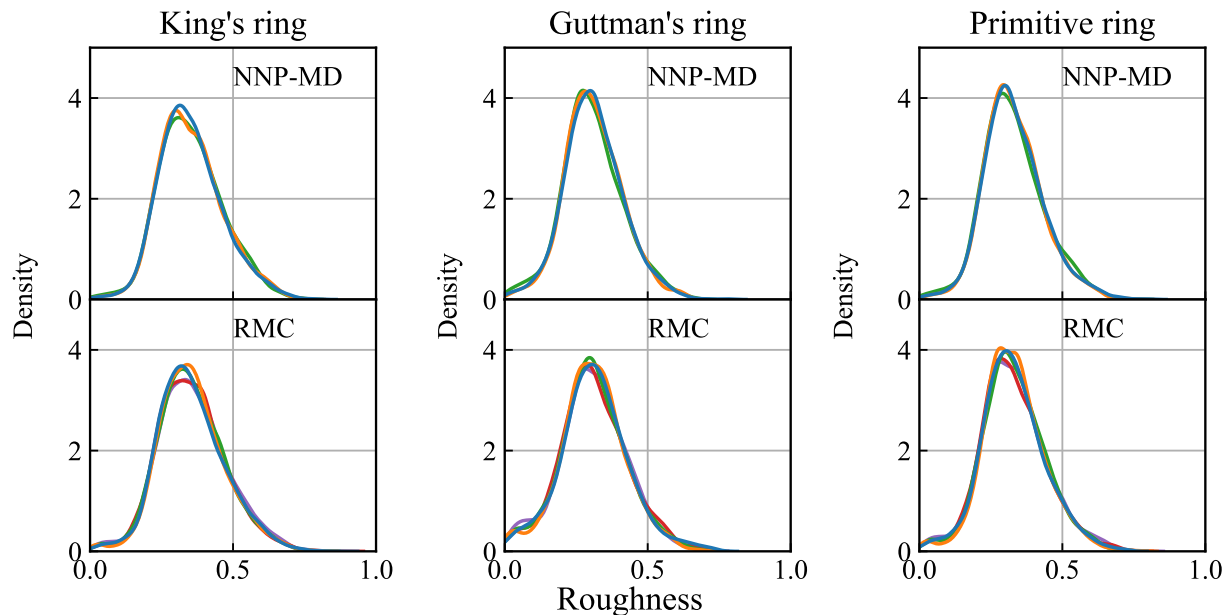


FIG. 7. Kernel density estimate plots of the roughness compared between NNP-MD and RMC using three ring definitions.

pairs around 0.8 \AA is broadened towards larger birth values in the RMC model compared to NNP models in line with the general tendency of RMC to favor more random structures as also seen in the bond angle and ring distributions above. On the other hand, NNP tend to strongly restrict covalent bond lengths, as implied by the small variation in the birth value of these islands.

Next, to further explore the differences between our models, the number of pairs present on the island over a death range of 2 \AA^2 to 7 \AA^2 and births range of 0.8 \AA^2 to 1.266 \AA^2 , which corresponds to the cutoff radius of the real space Ge-O bond length, was counted, yielding the results in Fig. 11. The RMC death distribution appears to be a bimodal distribution, with the first peak located around 2.5 \AA^2 and the second peak located around 3.75 \AA^2 . However, the NNP models only have a single sharp peak which is located around 3.5 \AA^2 . These behaviors appear similar to the results of traditional ring analysis, even though no ring definition is used, but unlike traditional ring distributions, differences can be seen on the length scales.

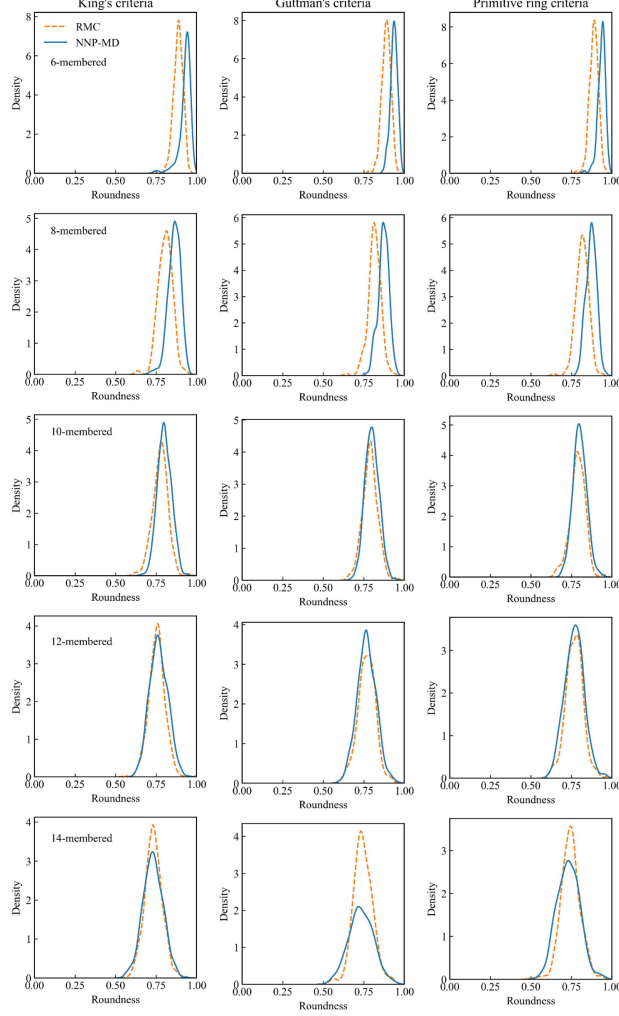


FIG. 8. Comparison between RMC (dashed lines) and NNP-MD (solid lines) results of roundness parameter results for each ring size (6- to 14-membered rings)

IV. SUMMARY

We constructed neural network potentials and performed extensive NNP-MD simulations to explore the structural features in glass structure and compared them with RMC analysis. The goal was to provide the real space image of intermediate-range order in the GeO_2 glass and evaluate the uncertainty of the RMC analysis based on simple constraints and neutron diffraction data, and our findings are summarized as follows:

- The structural models obtained from the NNP are in good agreement with the experimental results and the RMC analysis in terms of two-body correlations.

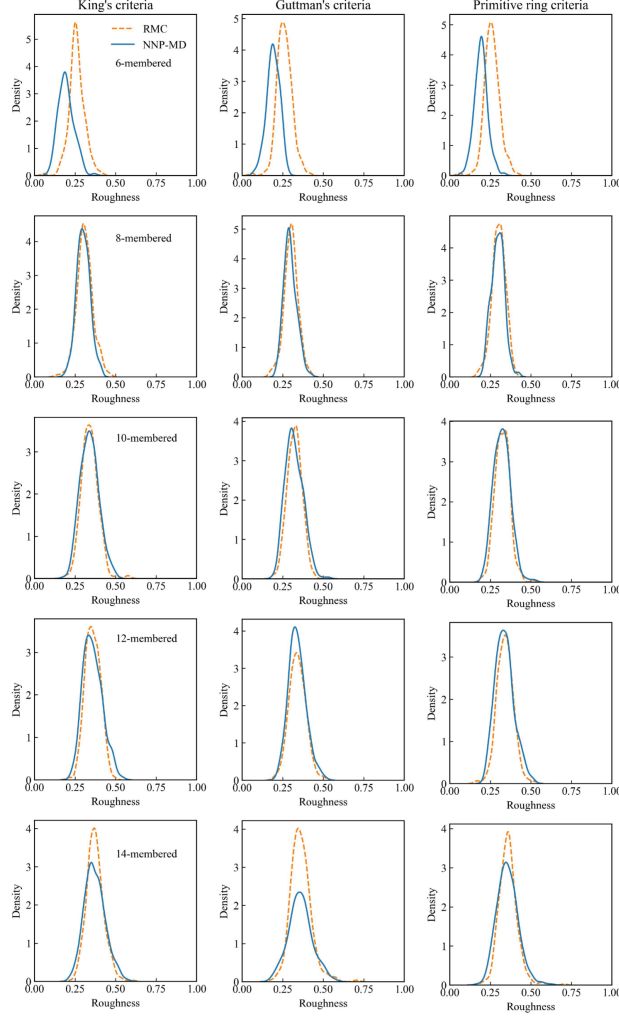


FIG. 9. Comparison between RMC (dashed lines) and NNP-MD (solid lines) results of roughness parameter results for each ring size (6- to 14-membered rings)

- Bond angle distributions are highly broadened in the RMC model compared to the NNP-MD model; this is in line with the well-known tendency of RMC to lead to more random structures.
- The intermediate range order as investigated by ring and topological data analysis leads to a sharper distribution in the NNP models and the underlying density functional method places stronger and probably more accurate restrictions on the intermediate range order in the glass structure.

In other words, the well-known shortcoming of relying only on two-body correlations for real-space modeling also affects the resulting intermediate-range order. This study demonstrates

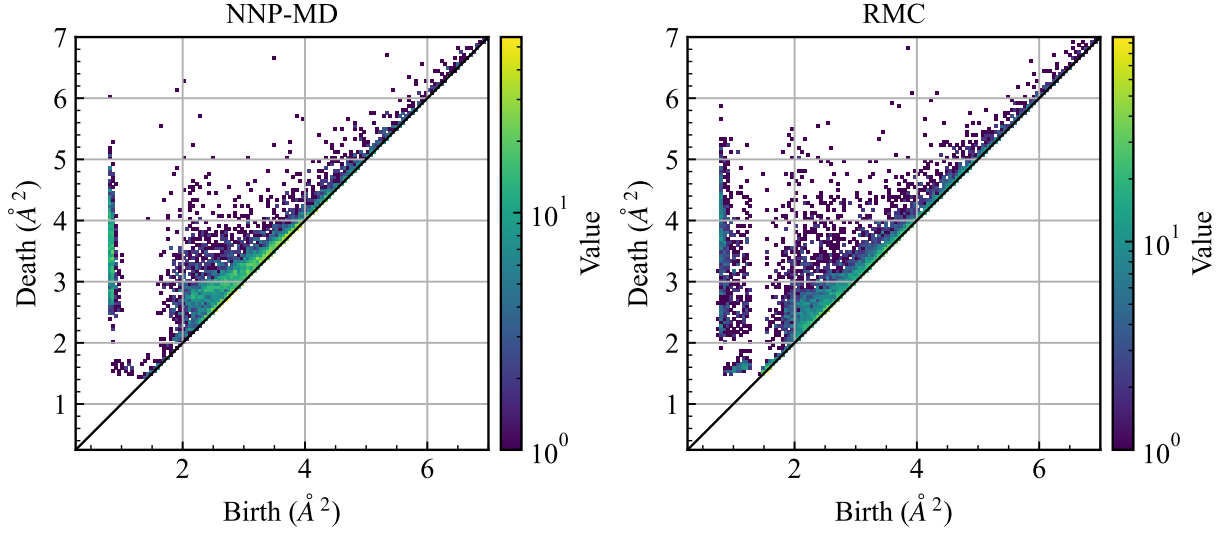


FIG. 10. The 1-dimensional persistence diagrams for each structure model, respectively.

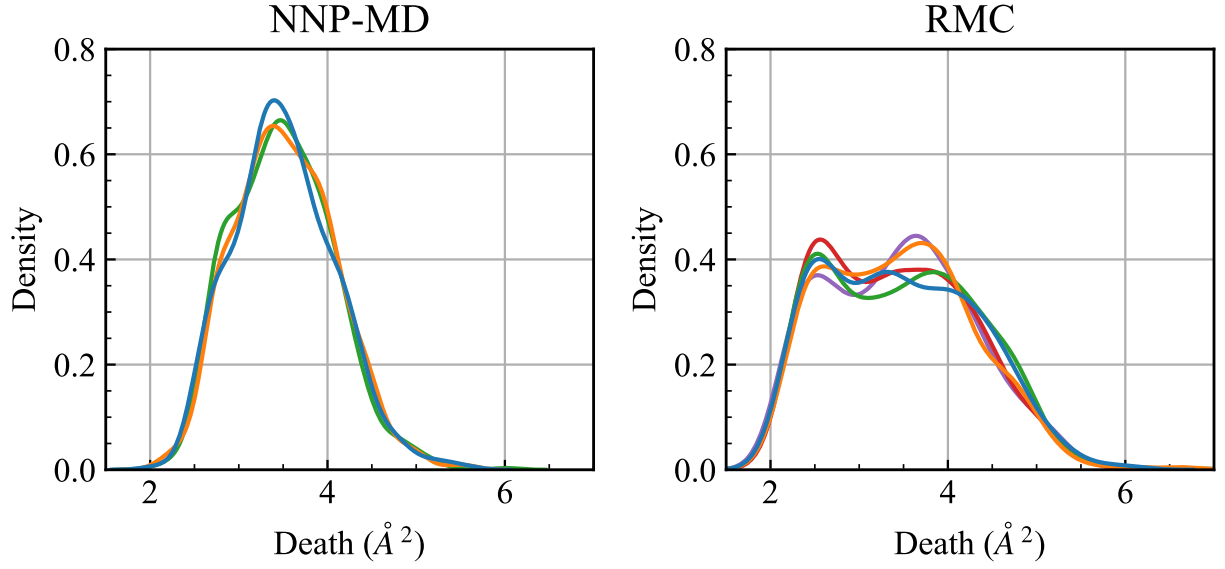


FIG. 11. Kernel density estimate plots of the distribution of death scales in restricted areas is described in the main text compared between NNP-MD and RMC results.

the promise of structural modeling with neural network potentials molecular dynamics for overcoming this issue.

ACKNOWLEDGMENTS

We would like to thank Philip Salmon for providing us with his neutron diffraction data, and Professor Motoki Shiga and Associate Professor Kazuto Akagi for their valuable advice on ring analysis and persistent homology. This research was financially supported by Japan Science and Technology Agency FOREST Program (Grant Number JPMJFR2037 Japan), supported by Japan Science and Technology Agency, the establishment of University fellowships towards the creation of science technology innovation, Grant Number JPMJFS2104 and also supported by the Japan Society for Promotion of Science (JSPS) KAKENHI Grant Number 20H02430. Computations were performed at the Super computer Center, ISSP, the Univ. of Tokyo.

AUTHOR DECLARATIONS

Conflict of Interest

The authors have no conflicts to disclose.

DATA AVAILABILITY

The datasets generated during this research are openly available from the ISSP Data Repository at <https://datarepo.mdcl.issp.u-tokyo.ac.jp>

REFERENCES

- ¹C. A. Angell, “Formation of Glasses from Liquids and Biopolymers,” *Science* (1995), 10.1126/science.267.5206.1924.
- ²M. F. Thorpe, “Continuous deformations in random networks,” *Journal of Non-Crystalline Solids* **57**, 355–370 (1983).
- ³A. Zeidler and P. S. Salmon, “Pressure-driven transformation of the ordering in amorphous network-forming materials,” *Phys. Rev. B* **93**, 214204 (2016).
- ⁴P. S. Salmon and A. Zeidler, “Ordering on different length scales in liquid and amorphous materials,” *J. Stat. Mech.* **2019**, 114006 (2019).

- ⁵Y. Onodera, S. Kohara, P. S. Salmon, A. Hirata, N. Nishiyama, S. Kitani, A. Zeidler, M. Shiga, A. Masuno, H. Inoue, S. Tahara, A. Polidori, H. E. Fischer, T. Mori, S. Kojima, H. Kawaji, A. I. Kolesnikov, M. B. Stone, M. G. Tucker, M. T. McDonnell, A. C. Hannon, Y. Hiraoka, I. Obayashi, T. Nakamura, J. Akola, Y. Fujii, K. Ohara, T. Taniguchi, and O. Sakata, “Structure and properties of densified silica glass: Characterizing the order within disorder,” *NPG Asia Materials* **12**, 1–16 (2020).
- ⁶P. S. Salmon, A. Zeidler, M. Shiga, Y. Onodera, and S. Kohara, “Ring compaction as a mechanism of densification in amorphous silica,” *Phys. Rev. B* **107**, 144203 (2023).
- ⁷P. H. Gaskell and D. J. Wallis, “Medium-Range Order in Silica, the Canonical Network Glass,” *Phys. Rev. Lett.* **76**, 66–69 (1996).
- ⁸C. Lin, L. E. Busse, S. R. Nagel, and J. Faber, “Temperature dependence of the structure factor of GeS₂ glass,” *Phys. Rev. B* **29**, 5060–5062 (1984).
- ⁹C. Massobrio and A. Pasquarello, “Origin of the first sharp diffraction peak in the structure factor of disordered network-forming systems: Layers or voids?” *The Journal of Chemical Physics* **114**, 7976–7979 (2001).
- ¹⁰D. A. Keen and R. L. McGreevy, “Structural modelling of glasses using reverse Monte Carlo simulation,” *Nature* **344**, 423–425 (1990).
- ¹¹G. Evrard and L. Pusztai, “Reverse Monte Carlo modelling of the structure of disordered materials with RMC++ : A new implementation of the algorithm in C++,” *J. Phys.: Condens. Matter* **17**, S1–S13 (2005).
- ¹²H. Morita, S. Kohara, and T. Usuki, “A new reverse Monte Carlo simulation code combined with molecular mechanics simulation (RMC–MM) for molecular and ionic liquids,” *Journal of Molecular Liquids* **147**, 182–185 (2009).
- ¹³K. V. Shanavas, N. Garg, and S. M. Sharma, “Classical molecular dynamics simulations of behavior of GeO₂ under high pressures and at high temperatures,” *Phys. Rev. B* **73**, 094120 (2006).
- ¹⁴D. Marrocchelli, M. Salanne, P. A. Madden, C. Simon, and P. Turq, “The construction of a reliable potential for GeO₂ from first principles,” *Molecular Physics* **107**, 443–452 (2009).
- ¹⁵X. F. Zhu and L. F. Chen, “First-principles molecular dynamics simulations of the structure of germanium dioxide under pressures,” *Physica B: Condensed Matter* **404**, 4178–4184 (2009).

- ¹⁶T. Li, S. Huang, and J. Zhu, “The structure and void analysis of pressure-induced amorphous GeO₂: Molecular dynamics simulation,” *Chemical Physics Letters* **471**, 253–257 (2009).
- ¹⁷K. Wezka, P. S. Salmon, A. Zeidler, D. A. J. Whittaker, J. W. E. Drewitt, S. Klotz, H. E. Fischer, and D. Marrocchelli, “Mechanisms of network collapse in GeO₂ glass: High-pressure neutron diffraction with isotope substitution as arbitrator of competing models,” *J. Phys.: Condens. Matter* **24**, 502101 (2012).
- ¹⁸S. S. Sørensen, C. A. N. Biscio, M. Bauchy, L. Fajstrup, and M. M. Smedskjaer, “Revealing hidden medium-range order in amorphous materials using topological data analysis,” *Sci. Adv.* **6**, eabc2320 (2020).
- ¹⁹L. C. Erhard, J. Rohrer, K. Albe, and V. L. Deringer, “A machine-learned interatomic potential for silica and its relation to empirical models,” *npj Comput Mater* **8**, 1–12 (2022).
- ²⁰K. Kobayashi, M. Okumura, H. Nakamura, M. Itakura, M. Machida, S. Urata, and K. Suzuya, “Machine learning molecular dynamics reveals the structural origin of the first sharp diffraction peak in high-density silica glasses,” *Sci Rep* **13**, 18721 (2023).
- ²¹M. Micoulaut, L. Cormier, and G. S. Henderson, “The structure of amorphous, crystalline and liquid GeO₂,” *J. Phys.: Condens. Matter* **18**, R753 (2006).
- ²²S. Kohara and K. Suzuya, “Intermediate-range order in vitreous SiO₂ and GeO₂,” *J. Phys.: Condens. Matter* **17**, S77 (2005).
- ²³K. Matsutani, A. Yamauchi, S. Kasamatsu, and T. Usuki, “Structural Analysis of Amorphous GeO₂ under High Pressure Using Reverse Monte Carlo Simulations,” *J. Phys. Soc. Jpn.* **91**, 124601 (2022).
- ²⁴O. Gereben and L. Pusztai, “RMC_POT: A computer code for reverse monte carlo modeling the structure of disordered systems containing molecules of arbitrary complexity,” *Journal of Computational Chemistry* **33**, 2285–2291 (2012).
- ²⁵Y. Onodera, S. Kohara, S. Tahara, A. Masuno, H. Inoue, M. Shiga, A. Hirata, K. Tsuchiya, Y. Hiraoka, I. Obayashi, K. Ohara, A. Mizuno, and O. Sakata, “Understanding diffraction patterns of glassy, liquid and amorphous materials via persistent homology analyses,” *Journal of the Ceramic Society of Japan* **127**, 853–863 (2019).
- ²⁶M. Shiga, A. Hirata, Y. Onodera, and H. Masai, “Ring-originated anisotropy of local structural ordering in amorphous and crystalline silicon dioxide,” *Commun Mater* **4**, 1–14 (2023).

- ²⁷S. R. Elliott, "Medium-range structural order in covalent amorphous solids," *Nature* **354**, 445–452 (1991).
- ²⁸J. C. Phillips, "Topology of covalent non-crystalline solids II: Medium-range order in chalcogenide alloys and A Si(Ge) - ScienceDirect," <https://www.sciencedirect.com/science/article/abs/pii/0022309381901721> (1981).
- ²⁹P. S. Salmon, "Real space manifestation of the first sharp diffraction peak in the structure factor of liquid and glassy materials," *Proceedings of the Royal Society of London. Series A: Mathematical and Physical Sciences* **445**, 351–365 (1994).
- ³⁰J. Behler, "First Principles Neural Network Potentials for Reactive Simulations of Large Molecular and Condensed Systems," *Angewandte Chemie International Edition* **56**, 12828–12840 (2017).
- ³¹J. Westermayr and P. Marquetand, "Machine Learning for Electronically Excited States of Molecules," *Chem. Rev.* (2020), 10.1021/acs.chemrev.0c00749.
- ³²S. Watanabe, W. Li, W. Jeong, D. Lee, K. Shimizu, E. Mimanitani, Y. Ando, and S. Han, "High-dimensional neural network atomic potentials for examining energy materials: Some recent simulations," *J. Phys. Energy* **3**, 012003 (2020).
- ³³J. Behler and M. Parrinello, "Generalized Neural-Network Representation of High-Dimensional Potential-Energy Surfaces," *Phys. Rev. Lett.* **98**, 146401 (2007).
- ³⁴N. Artrith, A. Urban, and G. Ceder, "Efficient and accurate machine-learning interpolation of atomic energies in compositions with many species," *Phys. Rev. B* **96**, 014112 (2017).
- ³⁵A. P. Bartók and G. Csányi, "Gaussian approximation potentials: A brief tutorial introduction," *Int. J. Quantum Chem.* **115**, 1051–1057 (2015).
- ³⁶R. Jinnouchi, J. Lahnsteiner, F. Karsai, G. Kresse, and M. Bokdam, "Phase Transitions of Hybrid Perovskites Simulated by Machine-Learning Force Fields Trained on the Fly with Bayesian Inference," *Phys. Rev. Lett.* **122**, 225701 (2019).
- ³⁷A. V. Shapeev, "Moment Tensor Potentials: A Class of Systematically Improvable Interatomic Potentials," *Multiscale Model. Simul.* **14**, 1153–1173 (2016).
- ³⁸D. Lee, K. Lee, D. Yoo, W. Jeong, and S. Han, "Crystallization of amorphous GeTe simulated by neural network potential addressing medium-range order," *Computational Materials Science* **181**, 109725 (2020).

- ³⁹S. V. King, “Ring Configurations in a Random Network Model of Vitreous Silica,” *Nature* **213**, 1112–1113 (1967).
- ⁴⁰L. Guttman, “Ring structure of the crystalline and amorphous forms of silicon dioxide,” *Journal of Non-Crystalline Solids* **116**, 145–147 (1990).
- ⁴¹K. Goetzke and H. J. Klein, “Properties and efficient algorithmic determination of different classes of rings in finite and infinite polyhedral networks,” *Journal of Non-Crystalline Solids* **127**, 215–220 (1991).
- ⁴²S. Le Roux and P. Jund, “Ring statistics analysis of topological networks: New approach and application to amorphous GeS₂ and SiO₂ systems,” *Computational Materials Science* **49**, 70–83 (2010).
- ⁴³Y. Hiraoka, T. Nakamura, A. Hirata, E. G. Escobar, K. Matsue, and Y. Nishiura, “Hierarchical structures of amorphous solids characterized by persistent homology,” *PNAS* **113**, 7035–7040 (2016).
- ⁴⁴I. Obayashi, T. Nakamura, and Y. Hiraoka, “Persistent Homology Analysis for Materials Research and Persistent Homology Software: HomCloud,” *J. Phys. Soc. Jpn.* **91**, 091013 (2022).
- ⁴⁵G. Kresse and J. Furthmüller, “Efficient iterative schemes for ab initio total-energy calculations using a plane-wave basis set,” *Phys. Rev. B* **54**, 11169–11186 (1996).
- ⁴⁶J. P. Perdew, K. Burke, and M. Ernzerhof, “Generalized Gradient Approximation Made Simple,” *Phys. Rev. Lett.* **77**, 3865–3868 (1996).
- ⁴⁷It is noted that the NNP trained on the data with lower cutoff and k-point mesh were not reliable when running long-time simulations and resulted in unphysical phase separation.
- ⁴⁸K. Lee, D. Yoo, W. Jeong, and S. Han, “SIMPLE-NN: An efficient package for training and executing neural-network interatomic potentials,” *Computer Physics Communications* **242**, 95–103 (2019).
- ⁴⁹J. Behler, “Constructing high-dimensional neural network potentials: A tutorial review,” *International Journal of Quantum Chemistry* **115**, 1032–1050 (2015).
- ⁵⁰N. Artrith and A. Urban, “An implementation of artificial neural-network potentials for atomistic materials simulations: Performance for TiO₂,” *Computational Materials Science* **114**, 135–150 (2016).
- ⁵¹D. P. Kingma and J. Ba, “Adam: A Method for Stochastic Optimization,” (2014).

- ⁵²S. Plimpton, “Fast Parallel Algorithms for Short-Range Molecular Dynamics,” *Journal of Computational Physics* **117**, 1–19 (1995).
- ⁵³A. P. Thompson, H. M. Aktulga, R. Berger, D. S. Bolintineanu, W. M. Brown, P. S. Crozier, P. J. in ’t Veld, A. Kohlmeyer, S. G. Moore, T. D. Nguyen, R. Shan, M. J. Stevens, J. Tranchida, C. Trott, and S. J. Plimpton, “LAMMPS - a flexible simulation tool for particle-based materials modeling at the atomic, meso, and continuum scales,” *Computer Physics Communications* **271**, 108171 (2022).
- ⁵⁴P. S. Salmon, “Order within disorder,” *Nature Mater* **1**, 87–88 (2002).
- ⁵⁵X. Yuan and A. N. Cormack, “Efficient algorithm for primitive ring statistics in topological networks,” *Computational Materials Science* **24**, 343–360 (2002).
- ⁵⁶<https://www.shiga-lab.org/sova>.
- ⁵⁷P. S. Salmon, A. C. Barnes, R. A. Martin, and G. J. Cuello, “Structure of glassy GeO₂,” *J. Phys.: Condens. Matter* **19**, 415110 (2007).
- ⁵⁸J. Akola, S. Kohara, K. Ohara, A. Fujiwara, Y. Watanabe, A. Masuno, T. Usuki, T. Kubo, A. Nakahira, K. Nitta, T. Uruga, J. K. R. Weber, and C. J. Benmore, “Network topology for the formation of solvated electrons in binary CaO–Al₂O₃ composition glasses,” *PNAS* **110**, 10129–10134 (2013).